Supporting Information

Table S1.Crystal data and structure refinement for *ct*-[RuCl(CO)(dppb)(bipy)]PF_6 **(1)** and *cc*-[RuCl(CO)(dppb)(phen)]PF_6 **(6).**

Table S2. Selected angles for for *ct*-[RuCl(CO)(dppb)(bipy)]PF_6 and *cc*-[RuCl(CO)(dppb)(bipy)]PF_6.

Table S3. Contributions, %, of the composing atoms in the frontier orbitals of the Ru-complexes *ct*-[RuCl(CO)(dppb)(bipy)]PF_6 (**1**), *tc*-[RuCl(CO)(dppb)(bipy)]PF_6 (**3**) and *cc*-[RuCl(CO)(dppb)(bipy)]PF_6 (**5**) calculated using the B3LYP/[Ru:SDD;C,H,P,N,Cl:6-311+G**] approach.

Table S4. Natural Bonding Orbitals (NBO) charges on the Ru and Ru-bound atoms of the complexes *tc*-[RuCl(CO)(dppb)(bipy)]PF_6 (**3**), *cc*-[RuCl(CO)(dppb)(bipy)]PF_6 (**5**), and *ct*-[RuCl(CO)(dppb)(bipy)]PF_6 (**1**), calculated using the B3LYP/[Ru:SDD;C,H,P,N,Cl:6-311+G**] approach.

Figure S1. (C) $^{13}C\{^1H\}$ NMR spectrum of *ct*-[RuCl(CO)(dppb)(bipy)]PF_6 complex in DMSO-d_6 at 300 K (A) Expanded regions of 110 – 200 ppm, (B) 5 – 30 ppm at different times.

Figure S2. (C) $^{13}C\{^1H\}$ NMR spectrum of *cc*-[RuCl(CO)(dppb)(bipy)]PF_6 isomer in DMSO-d_6 at 300 K, (A) Expanded regions of 120 – 210 ppm and (B) 21 – 31 ppm at different times.

Figure S3. (C) $^{13}C\{^1H\}$ NMR spectrum of *tc*-[RuCl(CO)(dppb)(bipy)]PF_6 complex in DMSO-d_6 at 300 K. (A) Expanded regions of 110 – 200 ppm and (B) 23 – 31 ppm at different times.

Figure S4. A) $^{31}P\{^1H\}$ NMR spectrum of solution after electrolysis of *ct*-[RuCl(CO)(dppb)(bipy)]PF_6 isomer in CH_3CN and B) cyclic voltammogram of the *ct*-[RuCl(CH_3CN)(dppb)(bipy)]PF_6 in CH_3CN.

Figure S5. A) $^{31}P\{^1H\}$ spectrum of solution after electrolysis of *tc*-[RuCl(CH_3CN)(dppb)(bipy)]PF_6 carried out for 3 h; B) cyclic voltammogram of *tc*-[RuCl(CH_3CN)(dppb)(bipy)]PF_6, C) ^{31}P NMR spectra of solution after electrolysis of *cc*-[RuCl(CO)(dppb)(bipy)]PF_6 for 4 h and D) cyclic voltammogram of *cc*-[RuCl(CH_3CN)(dppb)(bipy)]PF_6. Conditions: Pt electrode *vs* Ag/AgCl, TBAP 0.1 mol L^{-1} in CH_3CN.

Figure S6. $^{13}C\{^1H\}$ NMR spectra of electrolysis products. A) *ct*-[RuCl(CH_3CN)(dppb)(bipy)PF_6, B) *tc*-[RuCl(CH_3CN)(dppb)(bipy)]PF_6 and C) *cc*-[RuCl(CH_3CN)(dppb)(bipy)]PF_6 in DMSO-d_6.

Table S1.Crystal data and structure refinement for *ct*-[RuCl(CO)(dppb)(bipy)]PF_6 **(1)** and *cc*-[RuCl(CO)(dppb)(phen)]PF_6 **(6).**

Data	Complex (1)	Complex (6)
Empirical formula	$C_{39}H_{36}ClF_6N_2OP_3Ru$	$C_{41}H_{36}ClF_6N_2OP_3Ru$
Molecular weight	892.13	916.15
Color	Yellow	Yellow
Crystal system	Monoclinic	Monoclinic
Space group	P21/c	P21/c
Unit cell dimensions (Å; °)	a = 14.6581(2) b = 16.2338(2); c = 16.5500(2) β = 92.759(1)	a = 12.4950(4) Å b = 16.3401(6); c = 19.2663(6) β= 101.08
Volume ($Å^3$)	3933.62(9)	3860.2(2)
Unit cell, Z	4	4
Crystal size (mm^3)	0.22 x 0.22 x 0.19	0.05 x 0.09 x 0.40
Density (calculated; Mg/m^3)	1.506	1.576
Temperature (K)	293(2)	293(2)
Absorption coefficient (mm^{-1})	0.651	0.666
F(000)	1808	1856
Wavelength (Mo–Kα) (Å)	0.71073	0.71073
Theta range for data collection (°)	3.10 to 32.03	2.963 to 26.374
Index ranges	$-18 \leq h \leq 18$; $-20 \leq k \leq 20$; $-21 \leq l \leq 24$	-15<=h<=15; -20<=k<=20; -24<=l<=24
Completeness to theta	79.6 %	99.4 %
Reflections collected	10900	28914
Data / restraints / parameters	10900 / 478	7863 / 0 / 496
R1; wR2 [I>2σ (I)]	R1 = 0.0533, wR2 = 0.1388	R1 = 0.0589; wR2 = 0.1338
R1; wR2 (Total)	R1 = 0.0783, wR2 = 0.1659	R = 0.0589; R`= 0.1338
S	1.074	1.201
Largest diff. peak and hole	0.803 and -1.178	0.453 and -0.931

Table S2. Selected angles for for *ct*-[RuCl(CO)(dppb)(bipy)]PF_6 and *cc*-[RuCl(CO)(dppb)(phen)]PF_6.

ct-[RuCl(CO)(dppb)(bipy)]PF_6		*cc*-[RuCl(CO)(dppb)(phen)]PF_6	
Angles [°]		**Angles [°]**	
C(1)-Ru-N(1)	89.11(12)	C(1)-Ru-N(1)	169.54(14)
C(1)-Ru-N(2)	86.98(13)	C(1)-Ru-N(2)	91.79(14)
N(1)-Ru-N(2)	77.11(12)	N(2)-Ru-N(1)	77.93(11)
C(1)-Ru-P(1)	88.54(11)	C(1)-Ru-P(1)	94.87(12)
N(1)-Ru-P(1)	105.90(8)	N(2)-Ru-P(1)	89.79(9)
N(2)-Ru-P(1)	174.57(8)	N(1)-Ru-P(1)	87.14(8)
C(1)-Ru-Cl	94.91(11)	C(1)-Ru-P(2)	89.32(12)
N(1)-Ru-Cl	168.63(8)	N(2)-Ru-P(2)	170.33(9)
N(2)-Ru-Cl	92.46(9)	N(1)-Ru-P(2)	100.48(8)
P(1)-Ru-Cl	84.87(3)	P(1)-Ru-P(2)	99.68(3)
C(1)-Ru-P(2)	173.00(12)	C(1)-Ru-Cl	92.28(12)
N(1)-Ru-P(2)	92.54(7)	N(2)-Ru-Cl	83.27(9)
N(2)-Ru-P(2)	86.76(8)	N(1)-Ru-Cl	84.64(8)
P(1)-Ru-P(2)	97.53(3)	P(1)-Ru-Cl	170.19(3)
Cl-Ru-P(2)	82.24(3)	P(2)-Ru-Cl	87.09(3)
C(1)-Ru-P(2)	173.00(12)	C(1)-Ru-N(2)	91.79(14)
N(1)-Ru-P(2)	92.54(7)	C(1)-Ru-N(1)	169.54(14)

Table S3. Contributions, %, of the composing atoms in the frontier orbitals of the Ru-complexes *ct*-[RuCl(CO)(dppb)(bipy)]PF_6 (**1**), *tc*-[RuCl(CO)(dppb)(bipy)]PF_6 (**3**) and *cc*-[RuCl(CO)(dppb)(bipy)]PF_6 (**5**) calculated using the B3LYP/[Ru:SDD;C,H,P,N,Cl:6-311+G**] approach.

Species	HOMO	LUMO
(3) opt.	(C+H) 87	(C=O) 27; (C+H) 56
(5) opt.	(C+H) 93	(C=O) 11; (C+H) 82
(1) opt.	Ru: 54; Cl: 34; (C+H) 10	N: 20; (C+H) 77
(1) X-ray*	Ru: 58; Cl: 33	N: 17; (C+H) 80

**ct*-[RuCl(CO)(dppb)(bipy)]PF_6 complex calculated using X-ray coordinates.

Table S4. Natural Bonding Orbitals (NBO) charges on the Ru and Ru-bound atoms of the complexes *tc*-[RuCl(CO)(dppb)(bipy)]PF_6 (**3**), *cc*-[RuCl(CO)(dppb)(bipy)]PF_6 (**5**), and *ct*-[RuCl(CO)(dppb)(bipy)]PF_6 (**1**), calculated using the B3LYP/[Ru:SDD;C,H,P,N,Cl:6-311+G**] approach.

atoms	**complex 3 (opt.)**	**complex 5 (opt.)**	**complex 1 (opt.)**	**complex 1 (X-Ray)***
Ru	-1.38	-1.28	-0.66	-0.87
N1	-0.40	-0.69	-0.36	-0.36
N2	-0.35	-0.30	-0.37	-0.37
P1	2.79	1.01	1.20	1.30
P2	1.02	0.62	1.09	1.17
Cl	-0.27	-0.26	-0.40	-0.35
C(CO)	0.62	0.60	0.77	0.77
O	-0.50	-0.63	-0.44	-0.42

ct-[RuCl(CO)(dppb)(bipy)]PF_6 complex calculated using X-ray coordinates.

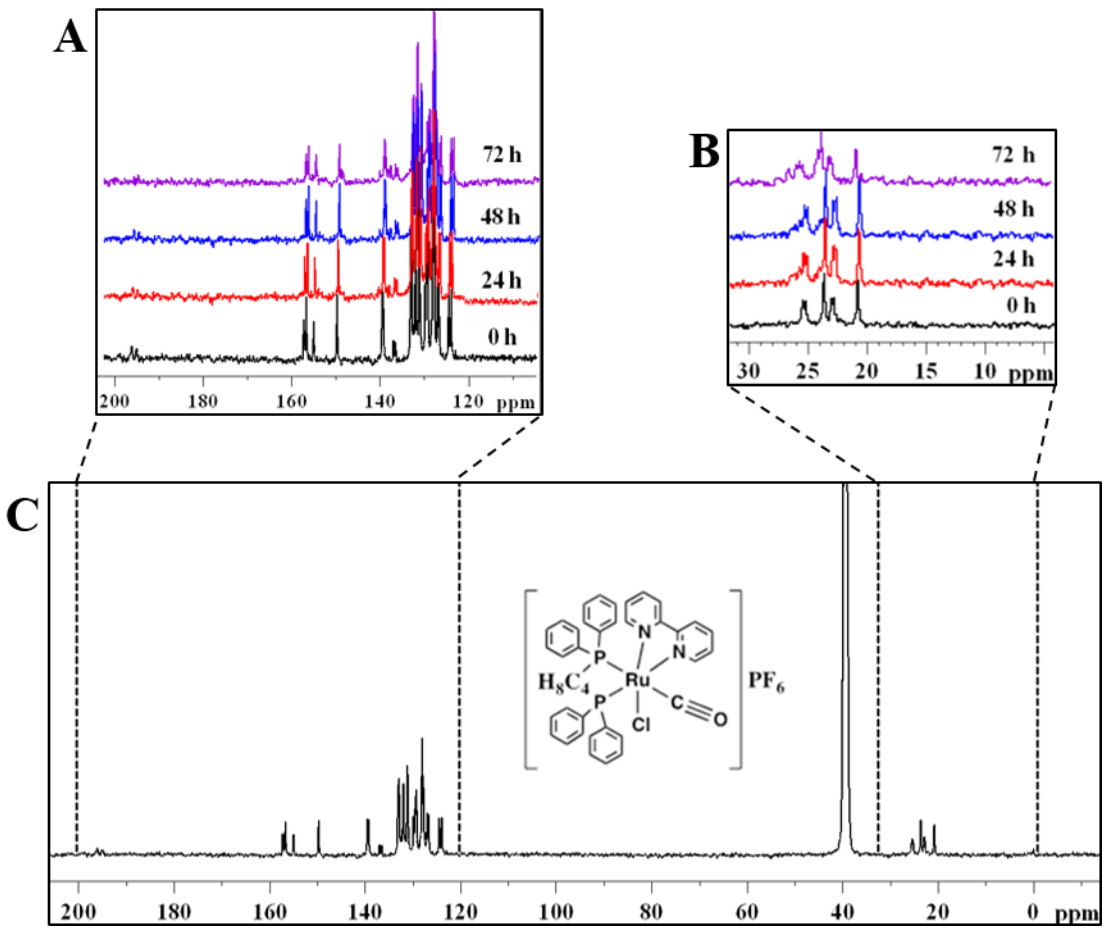

Figure S1. (C) $^{13}C\{^{1}H\}$ NMR spectrum of *ct*-[RuCl(CO)(dppb)(bipy)]PF_6 complex in DMSO-d_6 at 300 k (A) Expanded regions of 110 – 200 ppm, (B) 5 – 30 ppm at different times.

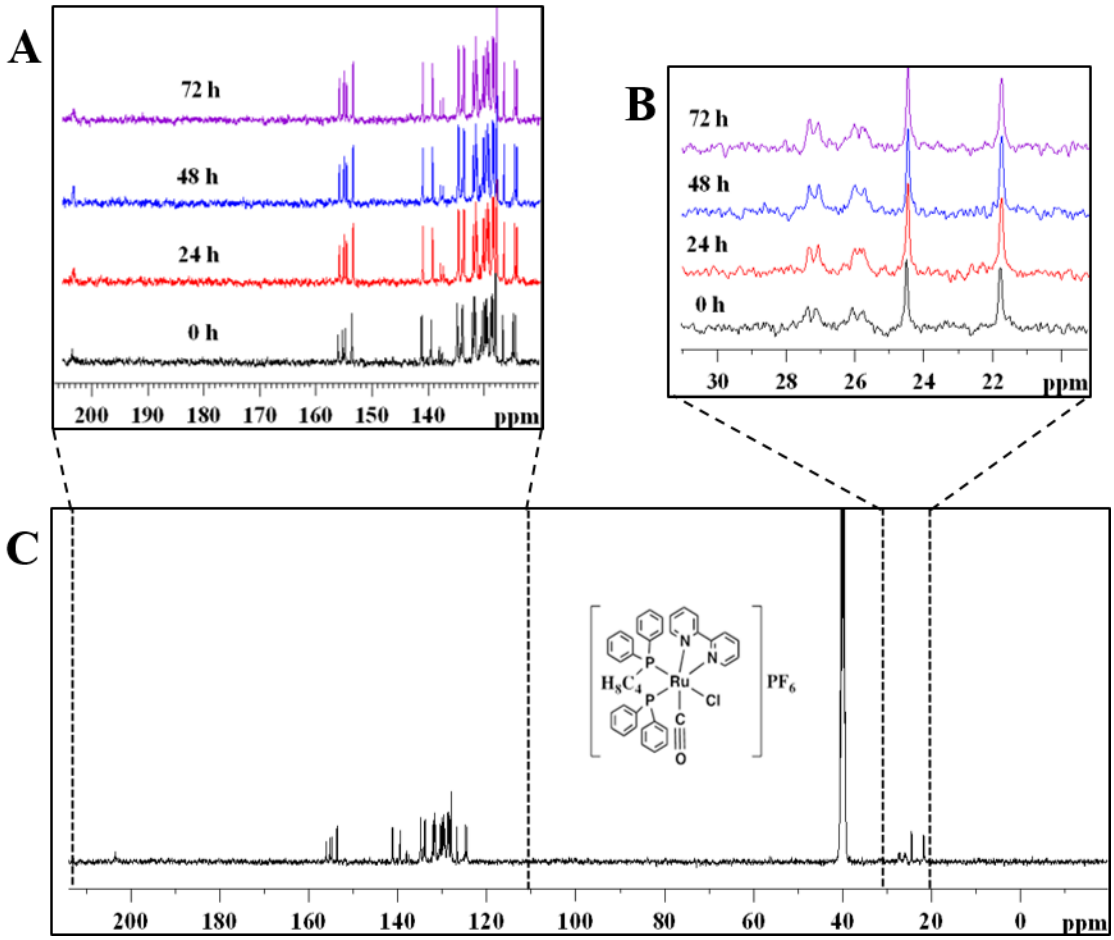

Figure S2. (C) $^{13}C\{^{1}H\}$ NMR spectrum of *cc*-[RuCl(CO)(dppb)(bipy)]PF_6 isomer in DMSO-d_6 at 300 K, (A) Expanded regions of 120 – 210 ppm and (B) 21 – 31 ppm at different times.

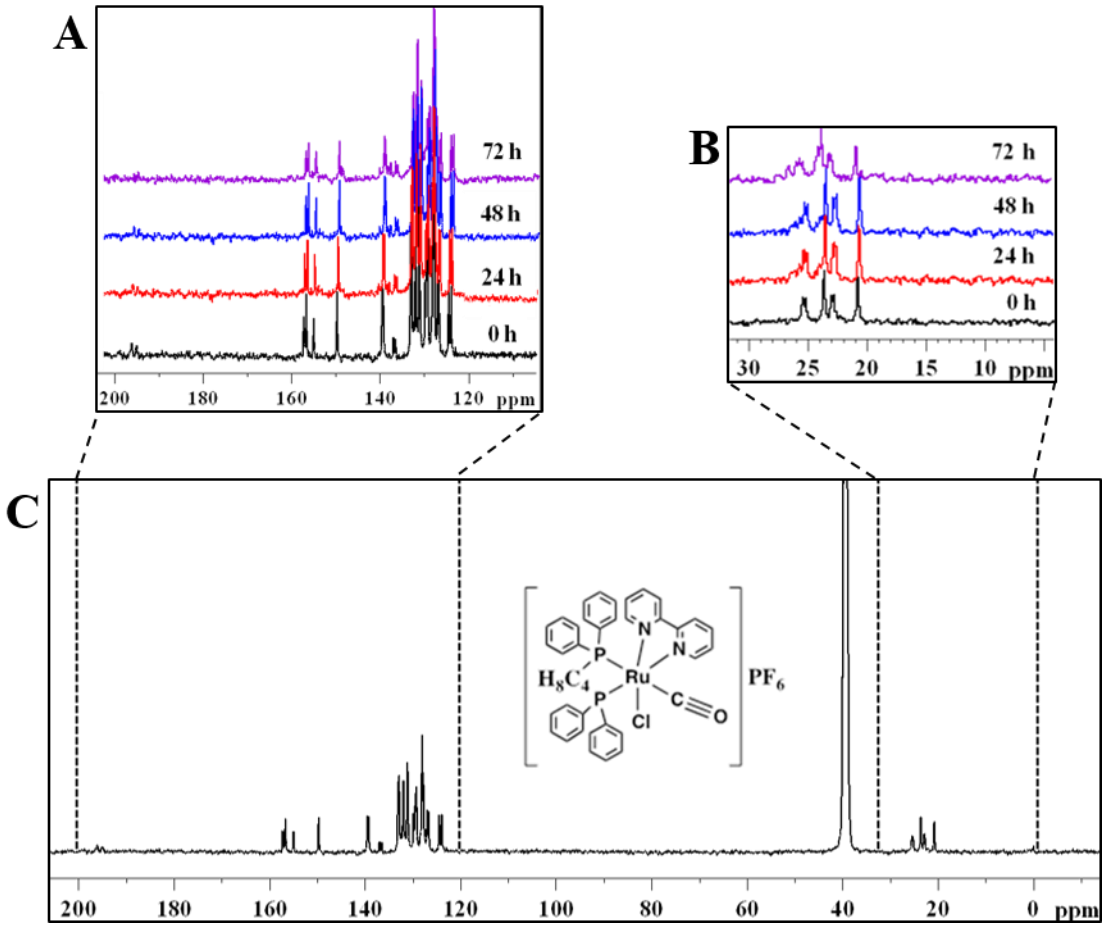

Figure S3. (C) $^{13}C\{^{1}H\}$ NMR spectrum of *tc*-[RuCl(CO)(dppb)(bipy)]PF_6 complex in DMSO-d_6 at 300 K. (A) Expanded regions of 110 – 200 ppm and (B) 23 – 31 ppm at different times.

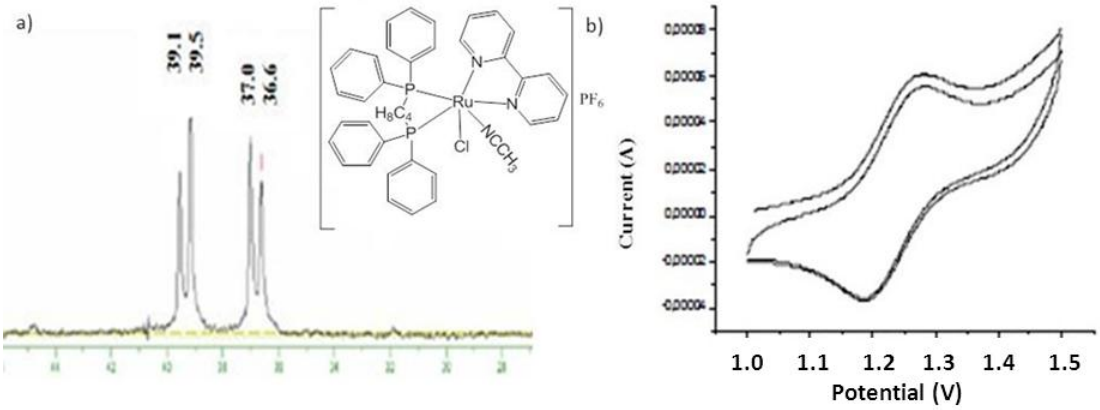

Figure S4. A) $^{31}P\{^{1}H\}$ NMR spectrum of solution after electrolysis of *ct*-[RuCl(CO)(dppb)(bipy)]PF_6 isomer in CH_3CN and B) cyclic voltammogram of the *ct*-[RuCl(CH_3CN)(dppb)(bipy)]PF_6 in CH_3CN.

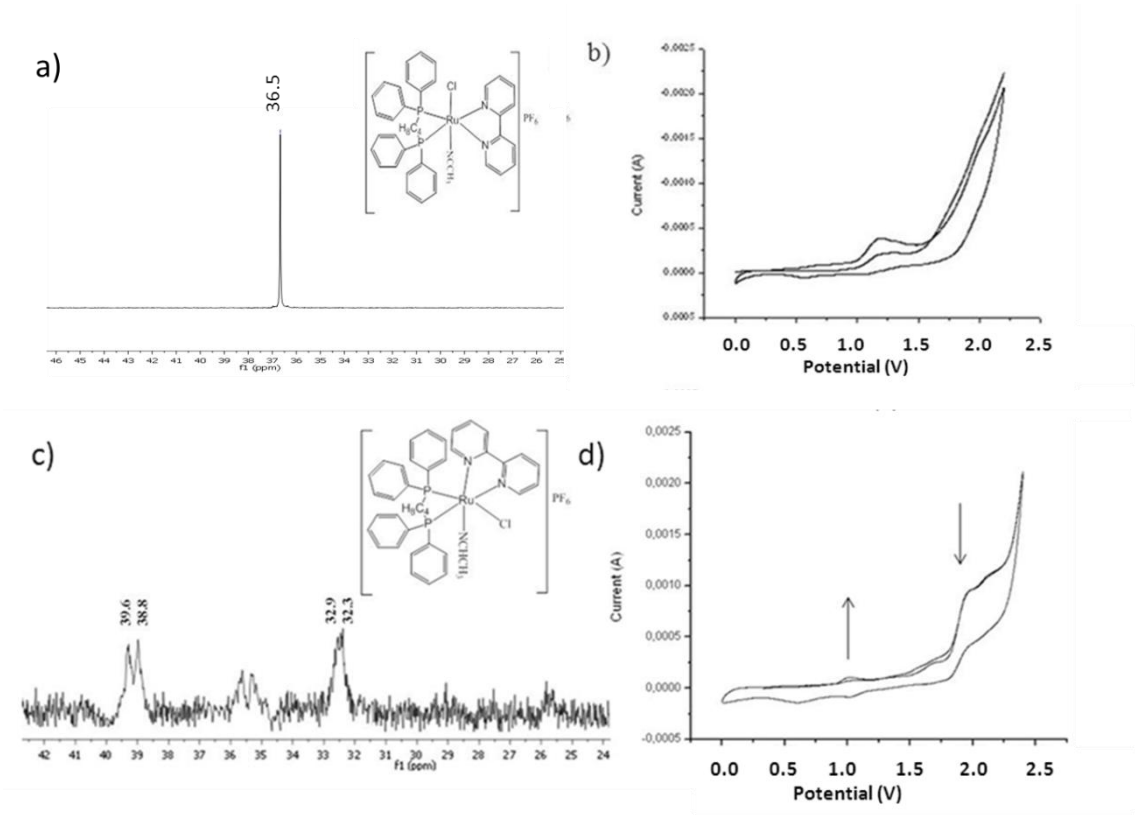

Figure S5. A) $^{31}P\{^{1}H\}$ spectrum of solution after electrolysis of *tc*-[RuCl(CH_3CN)(dppb)(bipy)]PF_6 carried out for 3 h; B) cyclic voltammogram of *tc*-[RuCl(CH_3CN)(dppb)(bipy)]PF_6, C) ^{31}P NMR spectra of solution after electrolysis of *cc*-[RuCl(CH_3CN)(dppb)(bipy)]PF_6 for 4 h and D) cyclic voltammogram of *cc*-[RuCl(CH_3CN)(dppb)(bipy)]PF_6. Conditions: Pt electrode *vs* Ag/AgCl, TBAP 0.1 mol L^{-1} in CH_3CN.

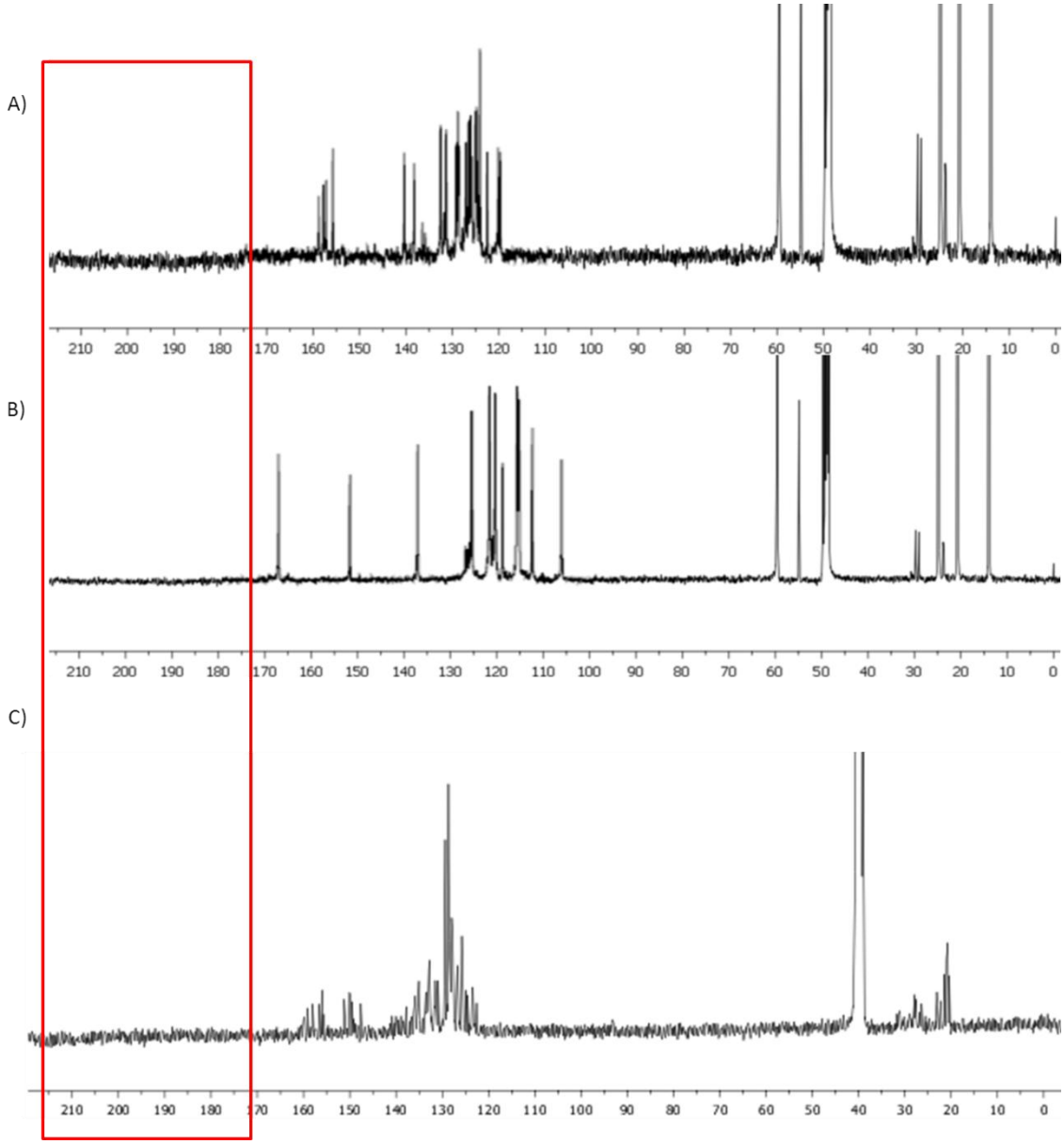

Figure S6. $^{13}C\{^{1}H\}$ NMR spectra of electrolysis products. A) *ct*-[RuCl(CH_3CN)(dppb)(bipy)]PF_6, B) *tc*-[RuCl(CH_3CN)(dppb)(bipy)]PF_6 and C) *cc*-[RuCl(CH_3CN)(dppb)(bipy)]PF_6.